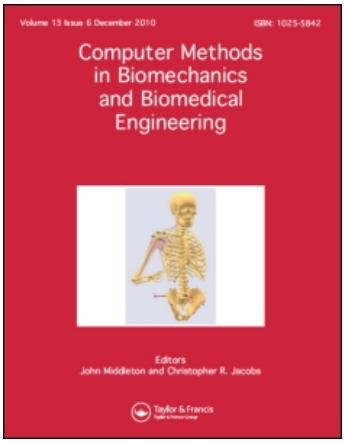

Computer Methods in Biomechanics and Biomedical Engineering
Publication details, including instructions for authors and subscription information:
http://www.informaworld.com/smpp/title~content=t713455284

A numerical model of the fracture healing process that describes tissue development and revascularisation

U. Simon[a]; P. Augat[a]; M. Utz[a]; L. Claes[a]
[a] Scientific Computing Centre Ulm, Institute of Orthopaedic Research and Biomechanics, University of Ulm, Ulm, Germany

First published on: 18 November 2010

To cite this Article Simon, U. , Augat, P. , Utz, M. and Claes, L.(2011) 'A numerical model of the fracture healing process that describes tissue development and revascularisation', Computer Methods in Biomechanics and Biomedical Engineering, 14: 1, 79 — 93, First published on: 18 November 2010 (iFirst)
To link to this Article: DOI: 10.1080/10255842.2010.499865
URL: http://dx.doi.org/10.1080/10255842.2010.499865

Computer Methods in Biomechanics and Biomedical Engineering
Vol. 14, No. 1, February 2011, 79–93

Taylor & Francis
Taylor & Francis Group

A numerical model of the fracture healing process that describes tissue development and revascularisation

U. Simon*, P. Augat, M. Utz and L. Claes

Scientific Computing Centre Ulm, Institute of Orthopaedic Research and Biomechanics, University of Ulm, Helmholtzstraße 20, 89081 Ulm, Germany

(*Received 2 September 2009; final version received 7 June 2010*)

A dynamic model was developed to simulate complex interactions of mechanical stability, revascularisation and tissue differentiation in secondary fracture healing. Unlike previous models, blood perfusion was included as a spatio-temporal state variable to simulate the revascularisation process. A 2D, axisymmetrical finite element model described fracture callus mechanics. Fuzzy logic rules described the following biological processes: angiogenesis, intramembranous ossification, chondrogenesis, cartilage calcification and endochondral ossification, all of which depended on local strain state and local blood perfusion. In order to evaluate how the predicted revascularisation depended on the mechanical environment, we simulated two different healing cases according to two groups of transverse metatarsal osteotomies in sheep with different axial stability. The model predicted slower revascularisation and delayed bony bridging for the less stable case, which corresponded well to the experimental observations. A revascularisation sensitivity analysis demonstrated the potential of the model to account for different conditions regarding the blood supply.

Keywords: mechanobiology; callus healing; tissue differentiation; perfusion; finite element; fuzzy logic

1. Introduction

Besides mechanical factors, the blood supply influences the process of secondary fracture healing (Pauwels 1960; Rhinelander 1968, 1974; Schweiberer and Schenk 1977; Hulth 1989; Claes et al. 1998). Revascularisation, tissue differentiation and local mechanical conditions depend on one another in a very complex manner. The formation of new bone tissue is only possible at locations with appropriate blood supply. Avascular regions need previous revascularisation before ossification processes can take place. An insufficient blood supply leads to a delayed healing or an atrophic non-union, even under appropriate mechanical conditions (Schweiberer and Schenk 1977; Perren and Rahn 1980). On the other side, a mechanically unstable situation is known to hinder the revascularisation process (Rhinelander 1974).

Numerical models of the fracture callus were developed to predict the pattern of mechanical stimuli in the healing tissue (Doblare et al. 2004), since it was not possible to measure them. Constant finite element (FE) models (Carter et al. 1988; Blenman et al. 1989; Cheal et al. 1991; Claes and Heigele 1999; Loboa et al. 2001; Gardner and Mishra 2003) predicted stress and strain distributions at particular healing stages of the fracture callus. Dynamic models (Ament et al. 1994, 1995; Ament and Hofer 2000; Kuiper et al. 2000; Bailon-Plaza and van der Meulen 2001, 2003; Lacroix and Prendergast 2002a, 2002b; Doblare et al. 2004; Geris et al. 2004, 2006, 2008; Gomez-Benito et al. 2005, 2006; Shefelbine et al. 2005; Isaksson et al. 2006a, 2006b, 2008; Garcia-Aznar et al. 2007) simulated the healing processes time-dependently using iterative loops. In most of these simulations, tissue differentiation and development depended on local mechanical signals like strain invariants (Bailon-Plaza and van der Meulen 2003; Doblare et al. 2004; Gomez-Benito et al. 2005, 2006; Garcia-Aznar et al. 2007; Isaksson et al. 2008) or the strain energy density (Ament and Hofer 2000). Poroelastic models used fluid velocity (Lacroix and Prendergast 2002a; Isaksson et al. 2008) or fluid shear stress (Kuiper et al. 2000) as mechanical stimuli in addition. Some models included biological factors like local concentrations of growth factors (Bailon-Plaza and van der Meulen 2001, 2003; Geris et al. 2006, 2008) or concentrations of different cell types (Bailon-Plaza and van der Meulen 2001, 2003; Lacroix and Prendergast 2002a, 2002b; Gomez-Benito et al. 2005, 2006; Garcia-Aznar et al. 2007; Geris et al. 2008; Isaksson et al. 2008). One approach also predicted callus growth in models with a changing FE mesh geometry using a thermoelastic analysis (Kuiper et al. 2000; Doblare et al. 2004; Gomez-Benito et al. 2005, 2006; Garcia-Aznar et al. 2007).

Most numerical models did not account for time-dependent revascularisation of the fracture callus, which is an important factor for osseous healing (Rhinelander 1974; Hulth 1989). One approach (Ament 1997) defined

*Corresponding author. Email: ulrich.simon@uni-ulm.de

ISSN 1025-5842 print/ISSN 1476-8259 online

DOI: 10.1080/10255842.2010.499865
http://www.informaworld.com

avascular and vascular tissue types, but did not include the vascularity as a separate state variable. This is necessary for modelling clinically relevant cases, such as compromised revascularisation due to peripheral soft tissue damage. Geris et al. (2008) developed a bioregulatory model based on the model of Bailon-Plaza and van der Meulen (2001) and made important extensions to describe angiogenesis interacting with other biological variables (growth factors, cell and tissue concentrations). Mechanical factors have not been included in this model.

Therefore, the aim of this study was to develop a dynamic mechanobiological fracture healing model that describes revascularisation in addition to tissue differentiation, using a spatio-temporal state variable to represent the local blood supply. Specifically, we wanted to evaluate (i) how predictions of revascularisation and tissue differentiation depend on differences in mechanical conditions at the fracture side. Additionally, we wanted to evaluate (ii) the sensitivity of model predictions to changes in the revascularisation parameters. Therefore, we simulated the healing of a diaphyseal osteotomy in an ovine metatarsus of two groups of different axial stability. We varied the revascularisation rate and calculated the course of interfragmentary movement (IFM). Predicted IFM were compared with measured movements of previous experiments in sheep (Claes et al. 1997) to confirm our model assumptions and to identify an appropriate revascularisation rate.

2. Materials and methods

The numerical model described the healing process in time t and space $\underline{x}$ using three main state variables:

$$\underline{C}(\underline{x},t) := \begin{bmatrix} \text{Blood perfusion} \\ \text{Cartilage concentration} \\ \text{Bone concentration} \end{bmatrix} = \begin{bmatrix} c_{\text{perf}}(\underline{x},t) \\ c_{\text{cart}}(\underline{x},t) \\ c_{\text{bone}}(\underline{x},t) \end{bmatrix}. \quad (1)$$

The space was limited to a constant healing domain Ω representing the potential fracture callus area.

(1) *Blood perfusion* $c_{\text{perf}}(\underline{x},t)$ was introduced as a state variable to enable the simulation of the complex interactions between revascularisation and tissue differentiation processes. It was designed to describe the extent of the local blood flow, providing the cells with oxygen, nutrients and growth factors, and enabling the transport of metabolic waste. This scalar variable was limited to values from 0% (no perfusion) to 100% (optimal for bone formation).

A changing mixture of the three basic tissue types (*soft tissue*, *fibrocartilage*, and *woven bone*) described the tissue differentiation processes within the healing domain. We used the local volumetric tissue concentrations of (2) *fibrocartilage* $c_{\text{cart}}(\underline{x},t)$ and (3) *woven bone* $c_{\text{bone}}(\underline{x},t)$ as main state variables, whereas the soft tissue concentration $c_{\text{soft}}(\underline{x},t)$ was just the complement to the sum of the other tissue concentrations to achieve 100%:

$$\sum_{\text{tiss}} c_{\text{tiss}} \stackrel{!}{=} 1, \quad \text{tiss} = (\text{soft}, \text{cart}, \text{bone}). \quad (2)$$

The evolution of the state variables $\underline{C}$ was in principle modelled as an initial value problem

$$\frac{\partial \underline{C}}{\partial t} = \underbrace{\underline{f}[\underline{C}, \underbrace{\underline{S}(\underline{C},F)}_{\substack{\text{Callus} \\ \text{mechanics}}}]}_{\text{Biological processes}}, \quad (3)$$

where the change in perfusion and tissue concentrations could be calculated from a complex functional $\underline{f}$ depending on the current state $\underline{C}$ of the tissue and the local mechanical stimuli $\underline{S}$. The stimuli vector $\underline{S}$ itself is also a complex functional, the solution of a boundary value problem (of elasticity) depending on the current tissue distribution $\underline{C}$ and the musculoskeletal load F. This is the mechanical part of the model. We solved it using the FE method (see Section 2.1 for more details). Because analytical expressions were not available for all mechanobiological processes, a rule-based method, i.e. the Fuzzy Logic, was chosen to describe the functional $\underline{f}$ (see Section 2.2 for more details).

In addition, the solution $\underline{C}(\underline{x},t)$ had to fulfil initial conditions at the starting time ($t_0 = 0$):

$$\underline{C}(0,\underline{x}) = \underline{C}_{\text{Init}}(\underline{x}) \quad (4)$$

and boundary conditions at the boundary Γ at $\underline{x} = \underline{x}_\Gamma$ (see Section 2.2 for more details):

$$\underline{C}(t,\underline{x}_\Gamma) = \underline{C}_{\text{Bound}}(t). \quad (5)$$

2.1 Mechanical part: FE model to determine the mechanical stimuli

A FE model (ANSYS, available from: www.ansys.com) described the mechanical behaviour of the fracture callus. The 2D, axisymmetric FE model was based on a standardised callus geometry (Claes and Heigele 1999) of an ovine metatarsus with a transverse osteotomy. We used the 'axisymmetry option' of the FE code instead of plane stress or plain strain option to enable a more realistic 3D stress and strain state. The FE mesh of 3758 elements represented one-half of a longitudinal section (Figure 1).

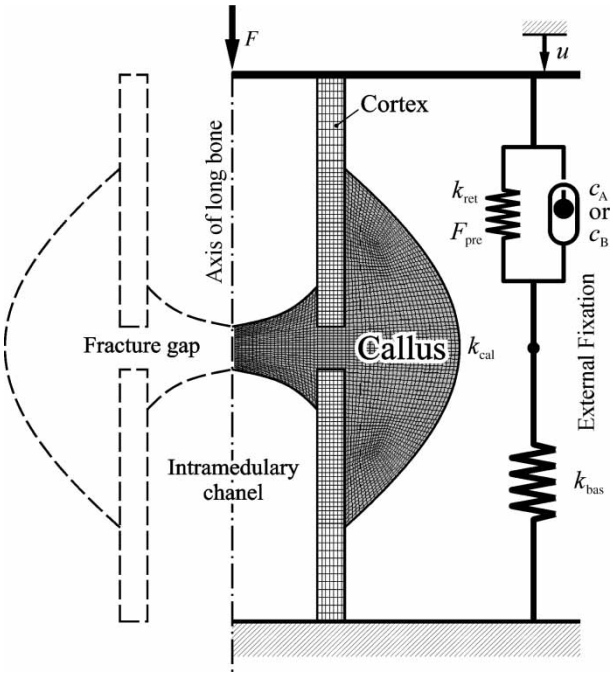

Figure 1. FE model (2D, axisymmetrical) of a standardised fracture callus geometry (callus stiffness k_{cal}, musculo-skeletal load F, IFM u) with a nonlinear fixation (basic stiffness k_{bas}, clearance c_A or c_B for case A or B, respectively, return spring with stiffness k_{ret} and pre-tension F_{pre}).

All FEs had linear elastic material properties. The cortex elements consisted of compact bone (Table 1), while the callus elements consisted of that changing tissue mixture (see above). Consequently, each callus element had its own material properties that were updated at each time step based on the current tissue concentrations and the properties of the pure tissues (Table 1). For the element's Young's modulus E_{el}, we took the tissue concentrations to the power of three as factors beside the tissue moduli:

$$E_{el} = \sum_{tiss} E_{tiss}\, c_{el,tiss}^3. \tag{6}$$

This equation is based on the experimental relation from Carter and Hayes (1977), where the apparent compressive modulus of trabecular bone specimens was proportional to the cube of their apparent bone density. For the element's Poisson's ratio ν_{el}, we used a linear rule of mixture:

$$\nu_{el} = \sum_{tiss} \nu_{tiss}\, c_{el,tiss}. \tag{7}$$

Initially, the callus tissue elements consisted of 100% soft tissue (0% cartilage and 0% bone).

Load and boundary conditions of the FE model were based on the previous animal experiment (Claes et al. 1997). The model was loaded in axial direction by a force of $F = 500$ N, which represents the amplitude of the major metatarsal loading during normal walking in sheep (Duda et al. 1998). The FE model was supported in axial direction at the distal end of the cortex. The nodes at the axis of rotational symmetry were fixed radially.

The external fixator used in the previously performed animal experiment (Claes et al. 1997) was designed to easily allow an axial movement of the fragments up to a predefined amount, while it was very rigid in all other directions (Claes et al. 1995). We described the axial nonlinear force–deflection behaviour (Figure 2) with a spring system (Figure 1) mounted in parallel to the callus consisting of a basic stiffness $k_{bas} = 4600$ N/mm, a clearance element c (adjustable), and a return spring (stiffness $k_{ret} = 20$ N/mm and pre-tension $F_{pre} = 100$ N; Claes et al. 1995).

Based on the tissue differentiation hypothesis of Pauwels (1960), we determined two independent strain invariants as mechanical stimuli

$$\underline{S} := \begin{bmatrix} \varepsilon_0 \\ \gamma_0 \end{bmatrix} \tag{8}$$

from the principal strains ε_1, ε_2, ε_3 of each element: the dilatational strain (hydrostatic strain) representing a

Table 1. Material properties of tissue types.

Tissue, tiss	Young's modulus, E_{tiss} (MPa)	Poisson's ratio, ν_{tiss}
Cortical bone	10,000	0.36
Woven bone	4000	0.36
Fibrocartilage	200	0.45
Connective tissue	3	0.30

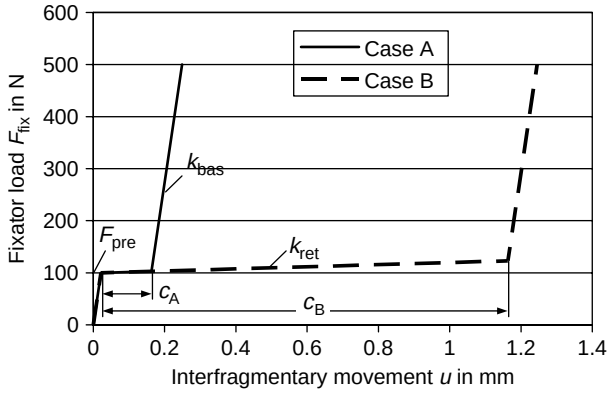

Figure 2. Nonlinear force–displacement function $F_{fix}(u)$ describing the mechanics of the external fixator (basic stiffness k_{bas}, clearance c_A or c_B for case A or B, respectively, return spring with stiffness k_{ret} and pre-tension F_{pre}).

volumetric change

$$\varepsilon_0 := \frac{1}{3}(\varepsilon_1 + \varepsilon_2 + \varepsilon_3) \tag{9}$$

and the distortional strain representing a change in shape

$$\gamma_0 := \frac{1}{\sqrt{2}}\sqrt{(\varepsilon_1 - \varepsilon_2)^2 + (\varepsilon_1 - \varepsilon_3)^2 + (\varepsilon_2 - \varepsilon_3)^2}. \tag{10}$$

2.2 Biological part: fuzzy logic controller

Fuzzy logic (Fuzzy Toolbox in Matlab (v6.0 R12), The MathWorks, Inc., Natick, MA, USA) was employed to simulate the biological processes. A Mamdani-type fuzzy logic controller (Mamdani and Assilian 1975; Kruse et al. 1994) predicted (deterministically) the changes in the state variables

$$\frac{\partial \underline{C}}{\partial t} = \text{fuzzy controller}[\underline{C}, \underline{C}_{\text{adj}}, \underline{S}] \tag{11}$$

(change in perfusion, change in cartilage concentration, change in bone concentration) depending on seven input variables. These were the three state variables $\underline{C}$ (perfusion, cartilage and bone concentration) themselves, two state variables in adjacent elements $\underline{C}_{\text{adj}}$ (perfusion and bone concentration in adjacent elements) and the mechanical stimuli $\underline{S}$ (dilatational and distortional strain; Figure 3).

The fuzzy controller consisted of eight linguistic if-then rules which described processes of angiogenesis, intramembranous ossification, chondrogenesis, cartilage calcification, endochondral ossification and tissue destruction (Table 2). Rules no. 1 and 2 represented angiogenesis of a FE with respect to local mechanical stimuli and perfusion of adjacent elements. Moderate strains and at least one neighbouring element with the same or a higher perfusion dictated an increase of the perfusion. A dilatational strain of an amount that corresponds to a hydrostatic stress (in connective tissue) larger than blood pressure was assumed to hinder the revascularisation process. Rule no. 3 described the intramembranous ossification. Areas with low mechanical stimuli and sufficient blood perfusion increased in bone concentration if at least one adjacent element had a high bone concentration. Rule no. 4 described chondrogenesis, which was possible with higher mechanical stimuli and low perfusion. Rule no. 5 represented the cartilage calcification, which occurred in the presence of higher mechanical stimuli and independently from perfusion. For the sake of simplicity, the increase of stiffness due to calcification was modelled with an increase of bone concentration and a decrease of cartilage concentration. Endochondral ossification (Rule no. 6) could occur under medium or high blood perfusion. Only completely calcified cartilage, which was characterised in our model by a high concentration of bone and a low concentration of cartilage, could undergo endochondral ossification. The rule, when active, predicted not only an increase in bone concentration but also a decrease in cartilage concentration of the same amount. Rules no. 7 and 8 modelled tissue atrophy due to mechanical overloading. When active, these rules predicted a rapid decrease in perfusion, cartilage concentration and bone concentration. Due to restrictions in the way rules could be defined in the Matlab fuzzy toolbox, we had to implement a total of 20 single rules.

Membership functions were defined for each of the seven fuzzy input (Figure 4) and the three fuzzy output variables (Figure 5). They related quantitative values (strains, concentrations, perfusion) to linguistic values (e.g. low, medium and high, increase) and vice versa. Trapezoidal functions for all linguistic values defined intervals, within the numerical values that belonged to them (Figures 4 and 5). The transition ranges at both sides of these functions predicted membership values smaller than one. This is the only reason why this approach has

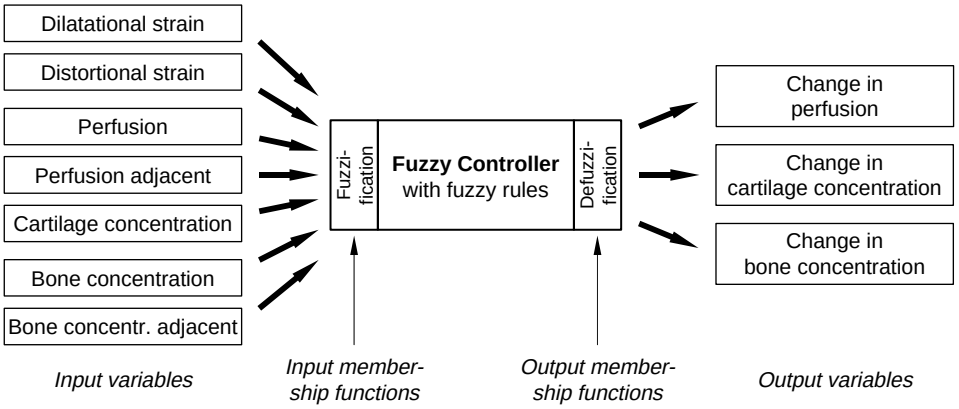

Figure 3. Fuzzy controller with seven fuzzy input and three fuzzy output variables. The controller includes fuzzification and defuzzification modules to transform numerical values into associated linguistic values and vice versa.

Table 2. Eight fuzzy rules describing biological processes of secondary fracture healing.

Fuzzy rules		IF input variable ...							... THEN output variable ...		
Process	No.	Perfusion	Perfusion, neighbour	Bone concentration	Bone concentration, neighbour	Cartilage concentration	Dilatational strain	Distortional strain	Change in perfusion	Change in bone concentration	Change in cartilage concentration
		... is ...							... has to ...		
Angiogenesis	1	Low	Medium or high	–	–	–	Neg. medium up to pos. high	Zero up to low	Increase	–	–
	2	Medium or high	High	–	–	–	Neg. medium up to pos. high	Zero up to low	Increase	–	–
Intramembr. ossification	3	High	–	–	High	Low	Neg. low or pos. low	Low	–	Increase	–
Chondro-genesis	4	–	–	–	–	–	Neg. medium up to neg. low	Not destructive	–	–	Increase
Cartilage calcification	5	–	–	–	Medium or high	Medium or high	Neg. medium up to pos. low	Zero up to medium	–	Increase	Decrease
Endochondral ossification	6	Medium or high	–	High	High	Low	Neg. low or pos. low	Zero up to low	–	Increase	Decrease
Atrophy	7	–	–	–	–	–	Neg. or pos. destructive	–	Decrease	Decrease	Decrease
	8	–	–	–	–	–	–	Destructive	Decrease	Decrease	Decrease

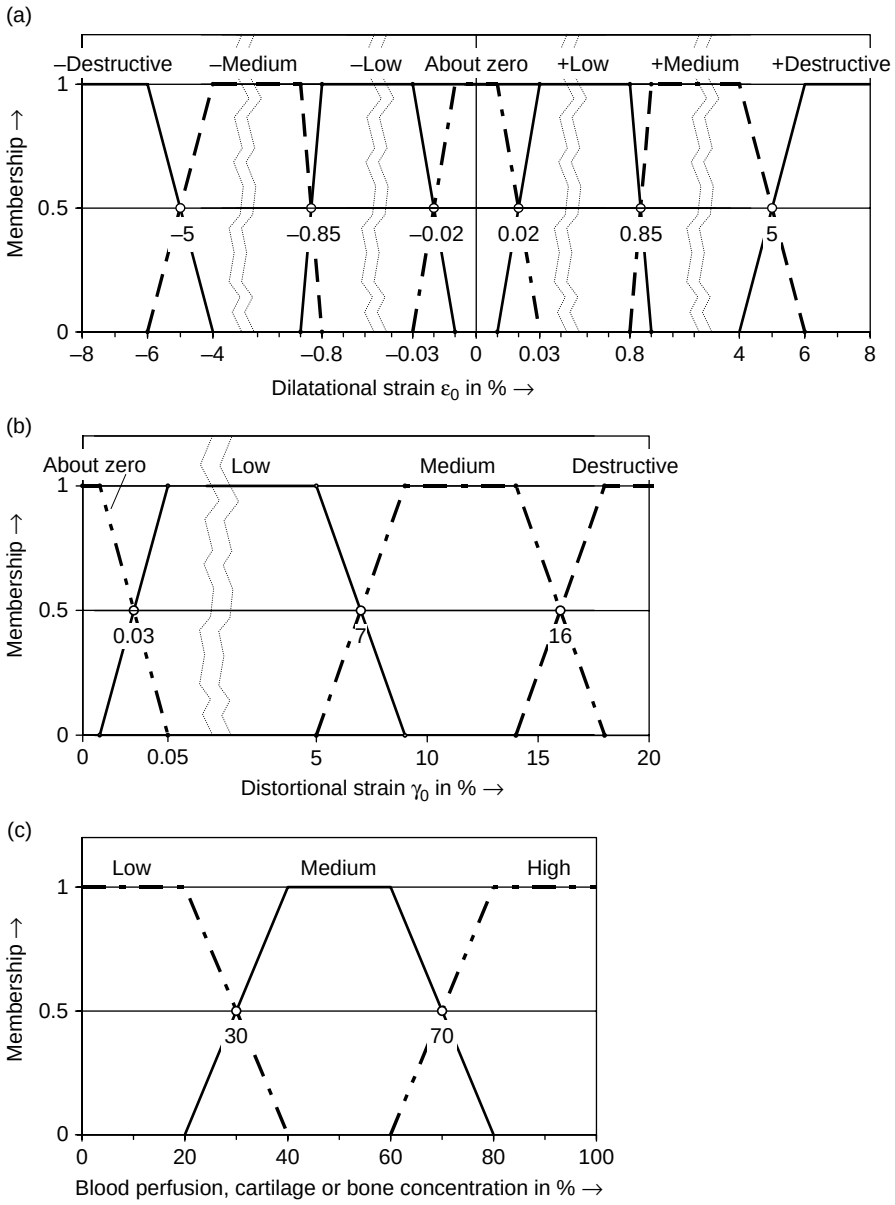

Figure 4. Membership functions for the seven fuzzy input variables: (a) dilatational strain, (b) distortional strain and (c) perfusion, perfusion in adjacent elements, cartilage concentration, bone concentration and bone concentration in adjacent elements.

to be called 'fuzzy' (membership functions with sharp edges would result in a 'sharp' logic). A particular strain value could be a 50%-member of the 'low' and a 50%-member of the 'high' strain state at the same time. Consequently, different rules could be active at the same time predicting possibly contrary outputs. The *centroid method* was used for the *fuzzy inference* procedure, which calculated the final output prediction as an averaged sum of the weighted single outputs of the active rules (Kruse et al. 1994).

Previous studies comparing the calculated strain patterns with histological results (Claes and Heigele 1999) as well as previous results of cell culture experiments (Kaspar et al. 2000) served as the basis for defining the membership functions (Figures 4 and 5) quantitatively. A previous study in sheep showed the sequence of new bone formation using markers at 4 weeks (calcein green) and 8 weeks (reverin; Claes and Heigele 1999). From the fluorescence images, we determined the maximum rate of new bone formation at $6.2\,\text{mm}/28\ \text{day} = 0.22\,\text{mm/day}$. This information was used to adjust the output membership function *change in bone concentration* (Figure 5). We assumed that this 'optimal' bone formation took place under optimal mechanical conditions. Consequently, bone formation could only be limited from the revascularisation

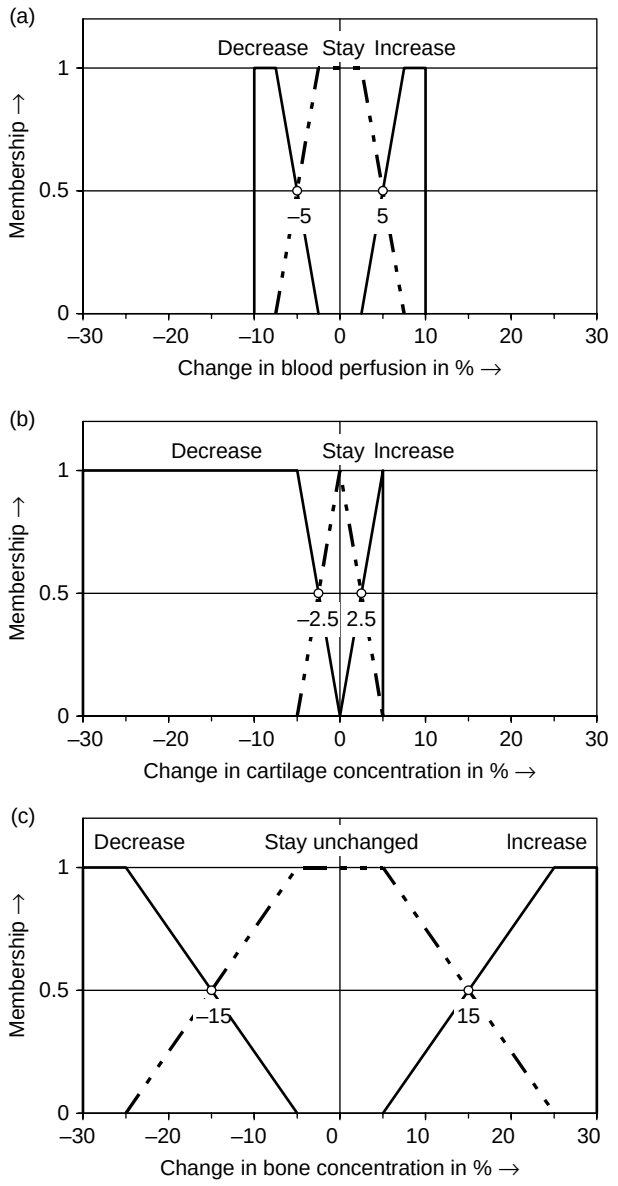

Figure 5. Membership functions for the three fuzzy output variables: (a) change in blood perfusion, (b) change in cartilage concentration and (c) change in bone concentration.

process. We, therefore, set the maximum revascularisation rate also to 0.22 mm/day as a first approximation.

Both the initial and boundary conditions for perfusion were defined to represent the experimental conditions. Cortex elements had optimal perfusion (100%), except for areas adjacent to the fracture. Those ends of the fragments (5 mm proximally and distally from the gap) had no initial perfusion (0%), because vessels maintaining these areas were typically ruptured (Rhinelander 1968, 1974). FEs with initially no perfusion (0%) characterised the avascular soft tissue (haematoma) of the initial callus. At the peripheral boundary of the callus, the perfusion was set to 30% in order to simulate the potential of an 'extraosseous blood supply' originating from adjacent soft tissues (Rhinelander 1974). At the boundary of the endosteal callus, the medullary channel perfusion was initially set to 0%. After 10 days, the perfusion boundary condition was set to 30% in order to represent the delayed potential of a revascularisation from the marrow (Rhinelander 1974).

2.3 Numerical implementation: iterative healing simulation

The callus healing process was described numerically as an initial value problem and was simulated time discretely using an iterative loop (Figure 6) over equidistant time steps (explicit Euler integration scheme):

$$\underline{C}_{i+1} = \underbrace{\frac{\partial \underline{C}}{\partial t}}_{\substack{\text{Fuzzy}\\ \text{output}}} \Delta t + \underline{C}_i. \tag{12}$$

The simulation started with a preprocessor run of the FE program, which generated geometry, element mesh, external fixation, load and boundary conditions. Initial values for the tissue composition, the material properties and the blood supply were assigned to each of the FEs representing the situation of the fractured bone immediately after fixation. Then, the iteration loop started with the FE analysis (FEA) to calculate the patterns of local mechanical stimuli (a special separation technique

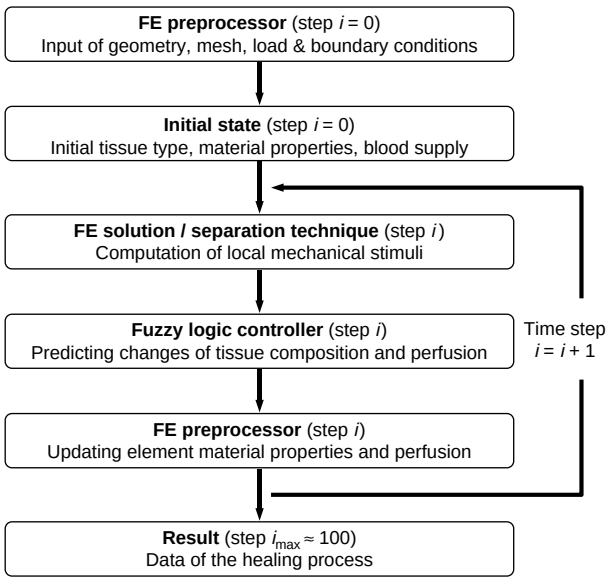

Figure 6. Flowchart of the dynamic fracture healing model including the FE method and the fuzzy logic in an iterative loop over time.

is described in more detail below). These stimuli together with the current tissue composition and local blood supply were used as input to the fuzzy logic controller. Fuzzy rules described changes in tissue composition and blood perfusion within each FE. A subsequent FE preprocessor run updated the material properties of the elements according to the new tissue compositions and the next iteration began. The simulation program was written using the ANSYS Parametric Design Language (APDL).

A separation technique ensured that the solution of our nonlinear iterative model could be obtained within a reasonable calculation time (<12 h). This formulation separated the nonlinear part of the FE model (fixator spring system) from the linear part (callus). At each time the procedure started with a linear FEA of the callus model without the fixator, yielding preliminary results. The callus was compressed by a unit displacement of $u_{\text{unit}} = 1$ mm prescribed to the most proximal nodes. The procedure determined the axial reaction force F_{unit} and subsequently the overall axial callus stiffness $k_{\text{cal}} = F_{\text{unit}}/u_{\text{unit}}$ at the particular time step i. The callus stiffness k_{cal} was then used to build the nonlinear force–displacement function for the entire system

$$F(u) = F_{\text{fix}}(u) + k_{\text{cal}} \cdot u \tag{13}$$

by the sum of fixator force $F_{\text{fix}}(u)$ (Figure 2) and callus force $k_{\text{cal}} \cdot u$. Using the inverted function $u(F)$, we calculated the actual interfragmentary displacement u_{act} resulting from the full load ($F = 500$ N) acting on the callus and fixator. The ratio of actual to unit displacement defined the scaling factor λ, which was then used to obtain the actual strain components $\varepsilon_{kl,\text{act}}$ from the preliminary calculated components $\varepsilon_{kl,\text{unit}}$:

$$\varepsilon_{kl,\text{act}} = \lambda \cdot \varepsilon_{kl,\text{unit}} \text{ with } \lambda := \frac{u_{\text{act}}}{u_{\text{unit}}} \text{ and } k, l = x, y, z. \tag{14}$$

2.4 Element size scaling and convergence analysis

Revascularisation and bone formation are kinds of surface growing processes: new bone tissue forms on existing bone surfaces only. Similar to this, a local increase in blood perfusion needs a good blood supply in the direct vicinity. Using the two additional fuzzy input variables *perfusion in adjacent elements* and *bone concentration in adjacent elements*, the fuzzy controller was able to consider these conditions. However, the fact that state variables were constant within elements and that state variable evolution was controlled by adjacent elements made the surface growth rates dependent on the mesh size (Figure 7). The distance from one element centre to the next (in the growing direction) was the factor influencing growth rates. Therefore, a further scaling was necessary to make the model independent of element size. The square

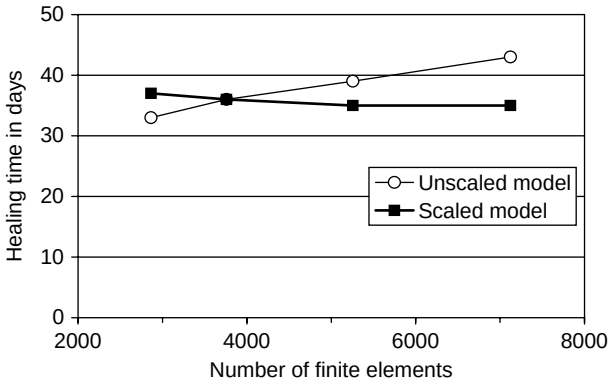

Figure 7. Convergence analysis. Influence of number of FEs on predicted healing time (time to bridge) for case A.

of the individual element area was used as an approximation of the local element centre distance to scale the fuzzy output as follows:

$$\begin{aligned} \Delta c_{\text{el,perf}} &= \sqrt{\frac{A_{\text{ref}}}{A_{\text{el}}}} \cdot \Delta c^{\text{fuzzy}}_{\text{el,perf}} \\ \Delta c_{\text{el,bone}} &= \sqrt{\frac{A_{\text{ref}}}{A_{\text{el}}}} \cdot \Delta c^{\text{fuzzy}}_{\text{el,bone}}, \end{aligned} \tag{15}$$

where A_{ref} is a reference area. A convergence analysis demonstrated that the influence of the mesh size was acceptably small for the entire healing model (Figure 7).

2.5 Sensitivity analysis

The revascularisation rate seemed to be a critical assumption. We varied this parameter in order to determine the sensitivity of the healing predictions to this variation. We used a preliminary definition of the output membership function *change in perfusion* (Figure 5(a)) which resulted in the maximum revascularisation rate of 0.22 mm/day (see assumption above). Then the predicted *change in perfusion* was scaled (in addition to element size scaling, see above) by a factor μ (0.5, 1.0 and 2.0) in order to vary the revascularisation rate. It should be mentioned that the maximum revascularisation rate under optimal conditions increased with an increasing scaling factor μ nonlinearly (Table 3). In an additional model variation, we assumed a permanent optimal perfusion for all elements (indicated by $\mu = \infty$). This represented a model which did not consider the revascularisation simulation at all.

2.6 Healing simulation and experimental evaluation

Using the numerical model, we simulated two different healing situations (cases A and B) corresponding to two experimental fracture healing cases in sheep (Claes et al. 1997). Briefly, this was an experimental study at the

Table 3. Results of sensitivity analyses: predicted healing time (bridging day) and maximum revascularisation rates resulting from different revascularisation factors μ.

Revascularisation factor (μ)	Max. revasc. rate (mm/day)	Bridging day	
		Case A	Case B
0.5	0.15	53	59
1.0	0.22	36	54
2.0	0.34	32	53
∞	∞	25	53

ovine metatarsus to compare the healing of a transverse osteotomy under different mechanical conditions as described below. Case A was the more stable group. The external fixator allowed a maximal IFM of 0.25 mm only. Case B, the less stable group, was characterised by a maximal IFM of 1.25 mm. The gap size in the loaded situation was 1.85 mm for both the cases. The gap sizes in the unloaded situations were 2.1 and 3.1 mm for case A and B, respectively. We compared the calculated course of the IFM with weekly measured axial movements of four individual sheep of each group from the previous experiment (Claes et al. 1997).

3. Results

The simulation predicted the distributions of all state variables (strains, element stiffness, perfusion, tissue concentrations) over both space and time. We present the results for dilatational strain, distortional strain, blood perfusion, bone concentration and fibrocartilage concentration for both the cases (A and B) at intervals of 14 days (Figures 8 and 9). The connective tissue concentration is the complement to bone and cartilage concentrations to achieve 100% and is, therefore, not presented.

The model predicted a delayed healing for the less stable case B. This case was characterised by larger mechanical stimuli. Highest absolute strain values were predicted in the interfragmentary gap during the initial healing phase and reached greater values for case B than for case A (Figure 8). As healing proceeds, the callus strains gradually decreased up to such physiological values as can be observed in the intact part of the cortical shell. Case B (day 56) reached this situation later than case A (at day 42; Figure 8).

We found a slower revascularisation process for the less stable case B. Revascularisation commenced from the peripheral side and from the cortex, and grew towards the centre of the periosteal callus for both the cases. Revascularisation of the avascular cortical ends occurred in both the cases with the same rate (Markers a and A in Figure 9). At day 14, the patterns of perfusion were similar for both the cases except that there was no revascularisation

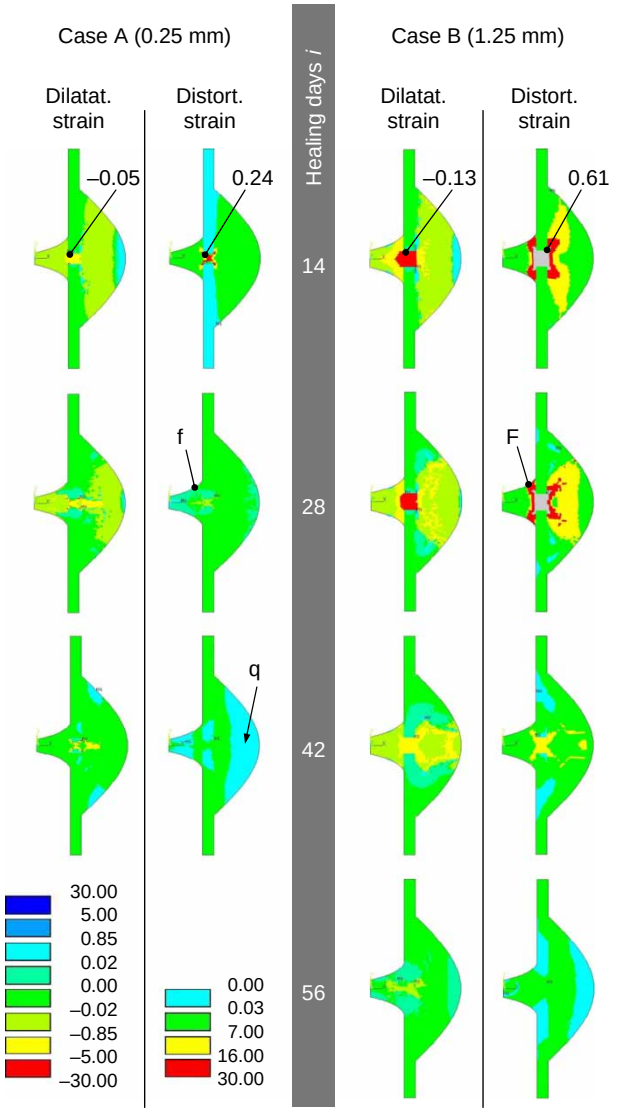

Figure 8. Predicted mechanical stimuli: dilatational and distortional strain in % for both the cases at healing day 14, 28, 42 and 56 (case B only). Highest absolute strain values (Marker) were predicted in the interfragmentary gap during the initial healing phase up to day 14. Non-uniform contour labels corresponding to intervals of membership functions (Figure 4(a) and (b)).

seen around the cortical ends close to the osteotomy for case B (Marker B vs. b). The perfusion boundary condition at the medullary edge was switched from 0 to 30% at day 10. Consequently, only a little perfusion could be found in this callus region at day 14 for both the cases (Markers c and C). At day 28, revascularisation of the periosteal callus was nearly complete for case A. In contrast, a large area in the centre of the periosteal callus remained without perfusion in case B (Marker D vs. d). Revascularisation of the internal callus proceeded for both the cases. For case B, the area next to the endosteum remained avascular (Marker E vs. e in Figure 9) due to higher distortional

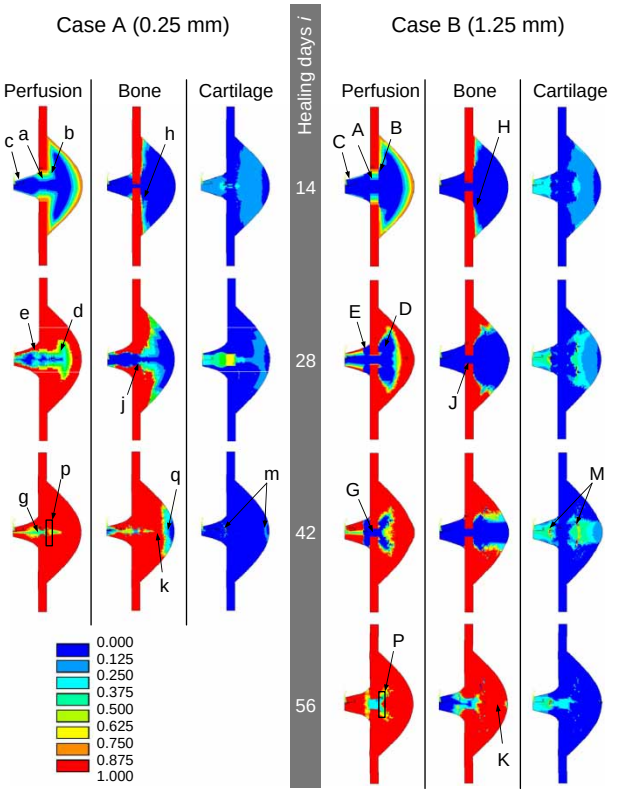

Figure 9. Predicted perfusion, bone and cartilage concentration for both the cases at healing day 14, 28, 42 and 56 (case B only). Vascularisation rate factor 1.0. Contour labels from 0% (dark blue) to 100% (red).

stains (Marker F vs. f in Figure 8). An avascular area between and around the fracture gap was found in case B up to day 42 (Marker G), whereas in case A, the interfragmentary area reached a perfusion of at least 39% (Marker g). The whole callus including the intercortical area was fully vascularised (100% perfusion) at day 51 for case A and at day 68 for case B (not shown in Figure 9).

Formation of new bone tissue was delayed for case B with more movement. The simulated healing process in both the cases commenced with intramembranous ossification. Bone formation started at the periosteal surface with some distance from the fracture gap. This distance was larger for case B with more movement than for case A (Marker H vs. h in Figure 9). Low strains, adequate blood supply and a bony surface as a prerequisite characterised this area of new bone formation. At day 28, new bone formed near the fracture site in the periosteal and endosteal callus for case A, but not for case B. Appositional bone formed in the fracture gap between the fragments for case A only (Marker j vs. J). During the healing process, the dominant type of ossification gradually changed from intramembranous to endochondral.

Bridging of new bone formation occurred later and more peripheral for the case of more movement. Bridging occurred in the peripheral callus at day 36 for case A and about 2 weeks later at day 54 for case B. The distance from the fracture gap to the bridging point (Positions k and K in Figure 9) was larger for case B. After bridging, the strains in the fracture gap decreased significantly, which enabled the ossification of the interfragmentary gap area.

The reduced stability in case B caused the predicted amount of fibrocartilage to increase. At day 28, we found areas of fibrocartilage formation in the periosteal and endosteal callus for both the cases. These areas experienced higher mechanical stimuli and less blood supply, and were larger for the less stable case B. Subsequently, the cartilage areas were reduced from the proximal and distal side by endochondral ossification. At day 42, the callus for case A contained almost no more cartilage (Marker m in Figure 9), whereas case B reached cartilage concentrations of up to 96% in the remaining gap (Marker M).

We compared the calculated course of IFM with the measured movements of four individual sheep of each group (Figure 11) of the previous animal experiment (Claes et al. 1997). The experimental curves showed a distinct period of rapid decrease in IFM, which was observed earlier for case A (around day 28) than for case B (around day 35). The predicted time courses captured these characteristic shapes for both the cases very well (Figure 11). Similar to the experiments, the model predicted periods of rapid decrease in IFM earlier for case A (days 21–33) than for case B (days 24–50).

The sensitivity analysis identified a strong influence of the revascularisation parameters on the predicted healing process. An increase of the revascularisation rate accelerated the healing process (Figures 10 and 12); bridging occurred earlier (Table 3). This effect was more pronounced in the stable case A, where patterns of new bone formation showed significant differences for different revascularisation parameters (images N vs. n in Figure 10). The compromised revascularisation ($\mu = 0.5$) delayed the healing by 17 days and the enhanced revascularisation ($\mu = 2.0$) accelerated the healing by 4 days compared with the standard revascularisation rate ($\mu = 1.0$). Without accounting for revascularisation, assuming an optimal blood supply from the first day onwards ($\mu = \infty$), healing time was further reduced.

In the less stable case B, the reduced revascularisation rate ($\mu = 0.5$) delayed the healing by only 5 days. An enhanced revascularisation ($\mu = 2.0$) and even the assumption of a permanent optimal blood supply ($\mu = \infty$) were not able to increase the healing speed compared with the standard revascularisation rate ($\mu = 1.0$; Figure 12, case B). Bone formation patterns for these cases of enhanced revascularisation (images O

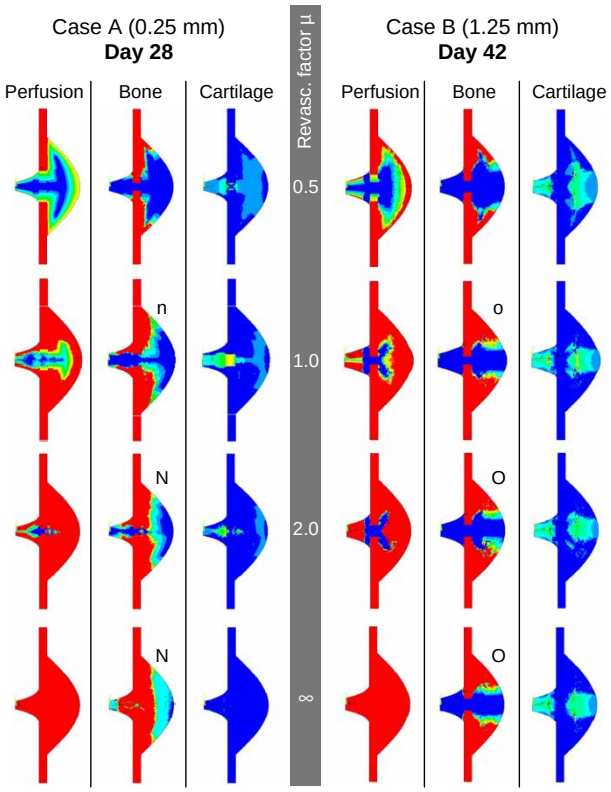

Figure 10. Results of sensitivity analysis: predicted perfusion, bone and cartilage concentration at healing time of rapid reduction in IFM (case A at day 28 and case B at day 42). Revascularisation factor 0.5 indicates compromised and 2.0 an enhanced revascularisation rate, while ∞ indicates optimal perfusion for all elements at all time steps. Contour labels (see Figure 9) from 0% (dark blue) to 100% (red).

in Figure 10) did not differ significantly from those of the standard case (image o).

Predicted IFM courses for the standard revascularisation parameter ($\mu = 1.0$) fitted best to the measured time courses (compare Figure 12 with Figure 11).

4. Discussion

The purpose of this study was to simulate the healing process of long bone fractures taking into account the local blood perfusion in addition to mechanical factors. In particular, we wanted to determine (i) how predicted revascularisation and subsequent ossification processes depend on mechanical conditions and (ii) the sensitivity of those predictions to variations in revascularisation parameters. We, therefore, developed a dynamic computer model using the method of fuzzy logic to model the revascularisation and differentiation processes; FEs described the callus mechanics. Using this model, we simulated the healing of a diaphyseal osteotomy in an ovine metatarsus of two groups of different axial stability. We calculated the time-dependent reduction of the IFM as an indicator for the healing process and analysed how this prediction depends on variations in the revascularisation parameters.

This simulation model has its particular strength in the consideration of the local blood perfusion. In addition to the mechanical situation, the blood supply is a very important factor for the osseous healing (Rhinelander 1974). While the chondrogenesis and the calcification of the fibrocartilage may precede the angiogenesis, intramembranous and endochondral ossification rely entirely on sufficient perfusion. Cartilage forms instead of woven bone if mechanical stimuli are inadequately large or local blood perfusion is too low for intramembranous ossification. The latter mechanism can only be modelled when considering the blood supply as an additional factor.

(i) The model predicted a delayed revascularisation and subsequently a delayed ossification for the less stable fracture fixation. The predicted revascularisation pattern showed characteristic features consistent to histological observations (Rhinelander 1974). Revascularisation emanated from all the three regions where potential blood sources were modelled in terms of boundary conditions,

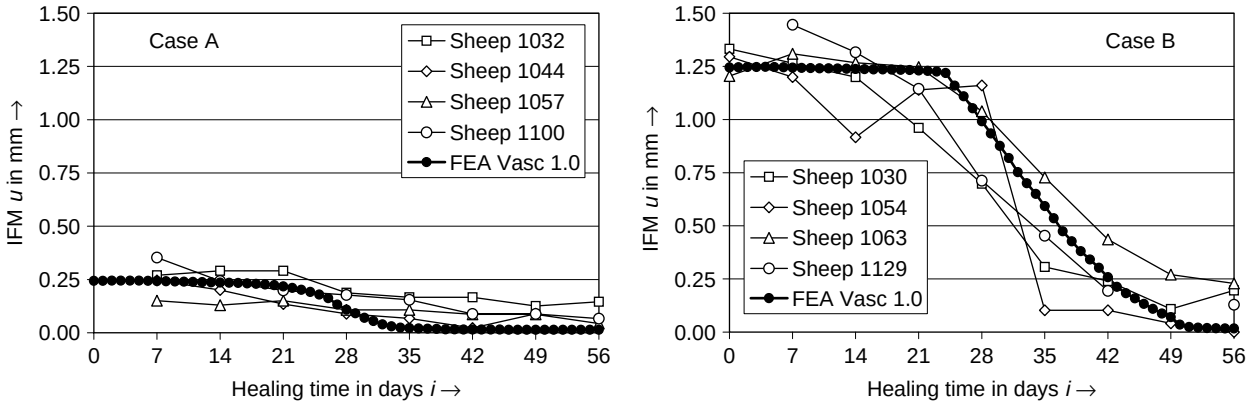

Figure 11. Course of axial IFM $u(t)$ over time. Weekly measured movements of four sheep of each group (Claes et al. 1997) in comparison with the respective FE predictions (vascularisation rate factor 1.0).

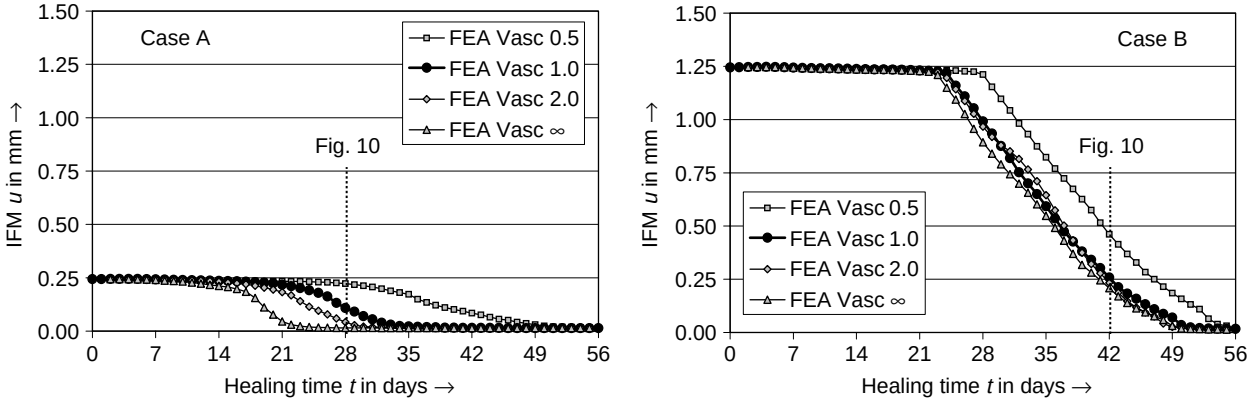

Figure 12. Results of sensitivity analysis. Predicted course of IFM $u(t)$ for different vascularisation rates. Factor 0.5 indicates compromised and 2.0 an enhanced revascularisation rate, while ∞ indicates optimal perfusion for all elements and time steps.

i.e. the 'medullary arterial supply', the vascularised part of the cortical bone, and the 'extraosseous blood supply' from peripheral soft tissues (Rhinelander 1974). Well vascularised areas grew towards the centre of the periosteal callus for both the cases, whereas regions of higher strains like the interfragmentary gap remained temporarily avascular. Within the displayed time frame of 42 days (case A) or 56 days (case B), the vascularisation did not reach the interfragmentary region completely, which is consistent with previous histological observations (Rhinelander 1974; Schweiberer and Schenk 1977). Blood vessels were not able to reach the central area between the fragments, before bridging of the peripheral callus occurred. In addition, a small line with very low perfusion persisted in the medullar callus. Previous histological studies (Rhinelander 1974; Schweiberer and Schenk 1977) also reported this effect. The reason for the delayed revascularisation of group B in the centre of the periosteal callus (Positions D vs. d in Figure 9) can mainly be seen in larger distortional strains, whereas the delay in the intercortical zone (Positions G vs. g in Figure 9) could be related to larger dilatational strains for the less stable case.

Claes et al. (2002) studied the blood vessel distribution in the fracture calluses of those experimental cases (A and B) our model is based on. The greatest differences in the vessel density between the groups were detected in the periosteal callus next to the cortical shell (Areas p and P in Figure 9). Significantly more vessels (mean values in vessels/mm^2) were seen in the more stable group A (plantar: 3.5; dorsal: 2.4) than for case B (plantar: 1.8; dorsal: 1.7). This result corroborated our numerical model, which similarly showed this characteristic difference in perfusion between the groups (Areas p vs. P in Figure 9).

The revascularisation delay resulted in a corresponding delay of ossification processes for case B, since blood perfusion is a prerequisite for the ossification. The bridging of new bone formation occurred about 2 weeks later and more peripherally for case B than for case A. Areas of connective tissue and fibrocartilage persisted at the central callus region and within the fracture gap. Consistent to histological results (Claes et al. 2002), the simulation predicted significantly more fibrocartilage in the fracture gap for group B with larger IFMs.

The gradual decrease of the calculated IFM correlated well with previous *in vivo* measurements (Claes et al. 1997) for both the cases. As long as the stiffness of the newly formed callus was lower than the stiffness of the external fixator k_{fix}, the movement did not change significantly. The differences in the initial IFM of the simulated cases were responsible for the characteristic differences in the healing response. Although our simulation predicted a healing delay for case B, the healing nevertheless succeeded until the end of the simulation process. The results of the *in vivo* experiments very similarly showed a successful healing for both the cases (Claes et al. 1997).

(ii) Predictions of revascularisation and tissue differentiation processes are sensitive to changes in the revascularisation parameters. Healing accelerated with an increasing revascularisation rate. This effect was smaller for case B where even the assumption of a permanent optimal blood supply was not able to increase the healing speed compared with the standard revascularisation rate. Only a further healing delay was seen when decreasing the revascularisation rate. This demonstrated that healing in the less stable case is primarily limited by an inadequate local mechanical environment, whereas the healing speed in the stable case depends mainly on the limited revascularisation rate.

When neglecting the revascularisation simulation, the model was not able to predict appropriate IFM time courses anymore. The model then predicted a too fast healing for the stable case. This divergence could be corrected by calibrating the model with a reduced ossification rate.

This calibration, however, would lead to a too slow healing prediction for the other case B. Only the model that considers revascularisation can be calibrated to predict healing times for both stable and unstable conditions.

With changes in the revascularisation parameters, the model presented in this study has the potential to account for different clinical phenomena. With a reduced revascularisation rate as demonstrated in the sensitivity analyses, the model can account for systemic factors compromising the revascularisation process (smoking, diabetes). Local factors like soft tissue damage or avascular fragments can be represented using reduced perfusion boundary conditions or reduced initial conditions, respectively. Future work is necessary to determine parameters for such cases quantitatively.

Another strength of the developed model is the formulation of the tissue adaptation and revascularisation with fuzzy logic rules. From a mathematical point of view, there is not a big difference to those models using ordinary differential equations (ODEs) of first order (Bailon-Plaza and van der Meulen 2001; Gomez-Benito et al. 2005; Geris et al. 2008; Isaksson et al. 2008). The fuzzy approach similar to the ODEs is fully determined. It can even be transformed into a nonlinear set of ODEs of the first order. The method of fuzzy logic, however, enables the integration of biological expertise as linguistic principles into the model. This makes this method easy to use even for those who are not familiar with ODEs. A robust fuzzy rule set can be setup up very fast. The linguistic rules can easily be discussed with medical or biological experts.

Despite its strengths, the model also has several limitations. Due to the assumption of rotational symmetry, the model cannot be used for oblique fractures or non-axisymmetrical load cases like bending and shear. We assumed homogeneous, linear elastic, isotropic properties for the different tissue types. This simplification seems to be acceptable since only small regions in the intercortical zone of the soft callus experienced critical strain levels. An exact prediction of these peak stresses and strains in this approach was not necessary because individual elements did not participate in healing processes until they experienced a low strain level. However, before applying these assumptions to other fracture healing cases (e.g. very small fracture gaps), one should carefully prove if the model will represent the overall force–displacement behaviour of the callus adequately. The musculoskeletal load was assumed to be constant over the healing time even though the animals were not able to fully bear the weight on their treated limbs in the first 2 weeks. This assumption was appropriate since the measured IFM indicated that the maximal possible movement was reached in the first weeks for both the groups (Figure 11). A further limitation of the model is the predefinition of the healing region. Callus tissues can never form outside from this region. It should represent the maximum potential healing region. To our opinion, the presence of peripheral tissues limits the size of the potential healing region in experimental and clinical cases too. On the other side, the stiff callus tissues (cartilage and woven bone) do not necessarily fill out the full region. The model therefore has in principle the potential to predict different callus sizes and shapes. In case A, 25% of the outer peripheral callus area was never filled with bone (Marker q in Figure 9), even not for much longer simulation times. After bridging, the mechanical stimuli in this area were too low for further bone formation (Marker q in Figure 8). For the accurate prediction of callus size and shape at later healing phases, bone resorption and remodelling from woven to lamellar bone should be considered. These processes were also neglected in this model. However, in order to predict healing in the first phases (up to callus bridging), the existing model seems to be adequate.

In contrast to previous models (Carter et al. 1988; Cheal et al. 1991; Claes and Heigele 1999), we used only strain and no stress variables as stimuli. Since the cells are embedded in an extracellular matrix, which is much stiffer than the cells themselves (Wang et al. 1993), internal forces are primarily transmitted through the extracellular matrix and not through the cells. Consequently, the cells are not able to directly detect the stress state of the tissue. The cells are rather able to sense the strain state via the deformation of their cavity. Cells might sense the flow or the hydrostatic pressure of a fluid phase surrounding them (which is not equal to the hydrostatic stress state of the tissue). Those signals, however, would be represented by the dilatational strain used in this work. Furthermore, it seems to be obvious that invariants of the strain tensor (dilatational and distortional strain) rather than components should be used to represent the mechanical stimuli, because cells cannot know about the orientation of any coordinate system.

In contrast to other healing models, we used a nonlinear rule of mixture to update the element moduli. Tissue concentrations to the power of 3 served as linear factors. This equation is based on the experimental relation from Carter and Hayes (1977), where the apparent compressive modulus of trabecular bone specimens was proportional to the cube of their apparent bone density. We used this equation, since woven bone is a structured mixture similar to trabecular bone. Experimental (Rice et al. 1988; Goldstein et al. 1991; Keyak et al. 1994) and theoretical studies (Winter 1993; Krstin et al. 2000; Hellmich and Ulm 2002) showed that a simple (linear) rule of mixture (as used by Ament and Hofer 2000; Lacroix and Prendergast 2002a, 2002b; Bailon-Plaza and van der Meulen 2003; Geris et al. 2004; Gomez-Benito et al. 2005; Isaksson et al. 2008) will certainly overestimate the apparent stiffness of a structured mixture like woven bone.

The results of this study demonstrated that only a model that describes both mechanical and biological

factors is able to predict the healing time for both stable and unstable conditions. All the fracture healing cases where the ossification is limited by the blood perfusion (systemic or local) can only be modelled adequately when considering this biological factor. With an extension to describe bone remodelling processes, the model was also able to describe fracture healing in trabecular bone (Shefelbine et al. 2005).

The new iterative simulation model of the fracture healing process allows us to simulate various mechanical conditions and differences in blood supply. It enables us to optimise the treatment methods and implants for fracture fixation and may reduce the need for animal experiments. Understanding of the dynamic interactions between tissue differentiation and vascularisation may help to explain the reasons for the delay of healing and the development of non-unions.

Acknowledgement

The German Research Foundation (Deutsche Forschungsgemeinschaft, DFG CL 77/7, CL 77/14) supported this work.

References

Ament C. 1997. Mathematische Modellbildung und Simulation der Knochenheilung [Dissertation]. Universität ulm. Fortschr.-Ber. VDI Reihe 17, Nr. 158, VDI Verlag.

Ament C, Hofer EP. 2000. A fuzzy logic model of fracture healing. J Biomech. 33(8):961–968.

Ament C, Hofer EP, Augat P, Claes L. 1994. Modeling of tissue transformation processes in fracture healing. Book of Abstracts, 4th Conference of the ISFR 94.

Ament C, Hofer EP, Augat P, Claes L. 1995. Fuzzy logic as a method to describe tissue adaption in fracture healing. Transactions of the 41st Annual Meeting of the Orthopaedic Research Society. p. 228.

Bailon-Plaza A, van der Meulen MC. 2001. A mathematical framework to study the effects of growth factor influences on fracture healing. J Theor Biol. 212(2):191–209.

Bailon-Plaza A, van der Meulen MC. 2003. Beneficial effects of moderate, early loading and adverse effects of delayed or excessive loading on bone healing. J Biomech. 36(8): 1069–1077.

Blenman PR, Carter DR, Beaupre GS. 1989. Role of mechanical loading in the progressive ossification of a fracture callus. J Orthop Res. 7(3):398–407.

Carter DR, Hayes WC. 1977. The compressive behavior of bone as a two-phase porous structure. J Bone Joint Surg Am. 59(7):954–962.

Carter DR, Blenman PR, Beaupre GS. 1988. Correlations between mechanical stress history and tissue differentiation in initial fracture healing. J Orthop Res. 6(5):736–748.

Cheal EJ, Mansmann KA, DiGioia AMD, Hayes WC, Perren SM. 1991. Role of interfragmentary strain in fracture healing: ovine model of a healing osteotomy. J Orthop Res. 9(1): 131–142.

Claes L, Heigele CA. 1999. Magnitudes of local stress and strain along bony surfaces predict the course and type of fracture healing. J Biomech. 32(3):255–266.

Claes L, Wilke HJ, Augat P, Rubenacker S, Margevicius KJ. 1995. Effect of dynamization on gap healing of diaphyseal fractures under external fixation. Clin Biomech (Bristol, Avon). 10(5):227–234.

Claes L, Augat P, Suger G, Wilke HJ. 1997. Influence of size and stability of the osteotomy gap on the success of fracture healing. J Orthop Res. 15(4):577–584.

Claes L, Heigele CA, Neidlinger-Wilke C, Kaspar D, Seidl W, Margevicius KJ, Augat P. 1998. Effects of mechanical factors on the fracture healing process. Clin Orthop Relat Res. (Suppl. 355):S132–S147.

Claes L, Eckert-Hubner K, Augat P. 2002. The effect of mechanical stability on local vascularization and tissue differentiation in callus healing. J Orthop Res. 20(5):1099–1105.

Doblare M, Garcia JM, Gomez MJ. 2004. Modelling bone tissue fracture and healing: a review. Eng Fract Mech. 71(1): 1809–1840.

Duda GN, Eckert-Hübner K, Sokiranski R, Kreutner A, Miller R, Claes L. 1998. Analysis of inter-fragmentary movement as a function of musculoskeletal loading conditions in sheep. J Biomech. 31(3):201–210.

Garcia-Aznar JM, Kuiper JH, Gomez-Benito MJ, Doblare M, Richardson JB. 2007. Computational simulation of fracture healing: influence of interfragmentary movement on the callus growth. J Biomech. 40(7):1467–1476.

Gardner TN, Mishra S. 2003. The biomechanical environment of a bone fracture and its influence upon the morphology of healing. Med Eng Phys. 25(6):455–464.

Geris L, Andreykiv A, Van Oosterwyck H, Sloten JV, van Keulen F, Duyck J, Naert I. 2004. Numerical simulation of tissue differentiation around loaded titanium implants in a bone chamber. J Biomech. 37(5):763–769.

Geris L, Gerisch A, Maes C, Carmeliet G, Weiner R, Vander Sloten J, Van Oosterwyck H. 2006. Mathematical modeling of fracture healing in mice: comparison between experimental data and numerical simulation results. Med Biol Eng Comput. 44(4):280–289.

Geris L, Gerisch A, Sloten JV, Weiner R, Oosterwyck HV. 2008. Angiogenesis in bone fracture healing: a bioregulatory model. J Theor Biol. 251(1):137–158.

Goldstein SA, Matthews LS, Kuhn JL, Hollister SJ. 1991. Trabecular bone remodeling: an experimental model. J Biomech. 24(Suppl. 1):135–150.

Gomez-Benito MJ, Garcia-Aznar JM, Kuiper JH, Doblare M. 2005. Influence of fracture gap size on the pattern of long bone healing: a computational study. J Theor Biol. 235(1): 105–119.

Gomez-Benito MJ, Garcia-Aznar JM, Kuiper JH, Doblare M. 2006. A 3D computational simulation of fracture callus formation: influence of the stiffness of the external fixator. J Biomech Eng. 128(3):290–299.

Hellmich C, Ulm FJ. 2002. Are mineralized tissues open crystal foams reinforced by crosslinked collagen? Some energy arguments. J Biomech. 35(9):1199–1212.

Hulth A. 1989. Current concepts of fracture healing. Clin Orthop Relat Res. 249:265–284.

Isaksson H, Wilson W, van Donkelaar CC, Huiskes R, Ito K. 2006a. Comparison of biophysical stimuli for mechano-regulation of tissue differentiation during fracture healing. J Biomech. 39(8):1507–1516.

Isaksson H, van Donkelaar CC, Huiskes R, Ito K. 2006b. Corroboration of mechanoregulatory algorithms for tissue differentiation during fracture healing: comparison with *in vivo* results. J Orthop Res. 24(5):898–907.

Isaksson H, van Donkelaar CC, Huiskes R, Ito K. 2008. A mechano-regulatory bone-healing model incorporating cell-phenotype specific activity. J Theor Biol. 252(2):230–246.

Kaspar D, Seidl W, Neidlinger-Wilke C, Ignatius A, Claes L. 2000. Dynamic cell stretching increases human osteoblast proliferation and cicp synthesis but decreases osteocalcin synthesis and alkaline phosphatase activity. J Biomech. 33: 45–51.

Keyak JH, Lee IY, Skinner HB. 1994. Correlations between orthogonal mechanical properties and density of trabecular bone: use of different densitometric measures. J Biomed Mater Res. 28(11):1329–1336.

Kruse R, Gebhardt J, Klawonn F. 1994. Foundations of fuzzy systems. New York: Wiley.

Krstin N, Nackenhorst U, Lammering R. 2000. Zur konstitutiven Beschreibung des anisotropen beanspruchungsadaptiven Knochenumbaus, Technische Mechanik 20:31–40.

Kuiper JH, Ashton BA, Richardson JB. 2000. Computer simulation of fracture callus formation and stiffness restauration. In: Proceedings of the 12th Conference of the European Society of Biomechanics; Dublin. p. 61.

Lacroix D, Prendergast P. 2002a. A mechano-regulation model for tissue differentiation during fracture healing: analysis of gap size and loading. J Biomech. 35(9):1163.

Lacroix D, Prendergast PJ. 2002b. Three-dimensional simulation of fracture repair in the human tibia. Comput Methods Biomech Biomed Eng. 5(5):369–376.

Loboa EG, Beaupre GS, Carter DR. 2001. Mechanobiology of initial pseudarthrosis formation with oblique fractures. J Orthop Res. 19(6):1067–1072.

Mamdani EH, Assilian S. 1975. An experiment in linguistic synthesis with a fuzzy logic controller. Int J Man–Machine Studies. 7(1):1–13.

Pauwels F. 1960. Eine neue Theorie über den Einfluß mechanischer Reize auf die Differenzierung der Stützgewebe. Z Anat Entwicklungsgeschichte. 121:478–515.

Perren SM, Rahn BA. 1980. Biomechanics of fracture healing. Can J Surg. 23(3):228–232.

Rhinelander FW. 1968. The normal microcirculation of diaphyseal cortex and its response to fracture. J Bone Joint Surg Am. 50(4):784–800.

Rhinelander FW. 1974. Tibial blood supply in relation to fracture healing. Clin Orthop. 105:34–81.

Rice JC, Cowin SC, Bowman JA. 1988. On the dependence of the elasticity and strength of cancellous bone on apparent density. J Biomech. 21(2):155–168.

Schweiberer L, Schenk R. 1977. Histomorphology and vascularization of secondary healing of bone fractures with emphasis on tibial shaft fracture (author's transl). Unfallheilkunde. 80(7):275–286.

Shefelbine SJ, Augat P, Claes L, Simon U. 2005. Trabecular bone fracture healing simulation with finite element analysis and fuzzy logic. J Biomech. 38(12):2440–2450.

Wang N, Butler JP, Ingber DE. 1993. Mechanotransduction across the cell surface and through the cytoskeleton. Science. 260(5111):1124–1127.

Winter W. 1993. Mechanics of damage and biomechanical tensile strength of the femur. Biomed Tech (Berl). 38(1–2): 10–13.